

Low cost wind energy conversion system based on the discontinuous conduction mode three-phase semi-controlled rectifier

ISSN 1755-4535

Received on 8th August 2014

Accepted on 2nd December 2014

doi: 10.1049/iet-pel.2014.0639

www.ietdl.org

Eduardo Façanha Oliveira¹, Fernando Lessa Tofoli², Fernando Marcelo Antunes¹, Luiz Henrique Silva Colado Barreto¹, Paulo Peixoto Praça¹, Demercil de Sousa Olivaira Júnior¹ ✉

¹Department of Electrical Engineering, Federal University of Ceara, Campus do Pici, Av. Mister Hall, s/n, Fortaleza 60455-760 Ceará, Brazil

²Department of Electrical Engineering, Federal University of São João del-Rei, Praça Frei Orlando, 170 – Centro, Campus Santo Antonio, São João del-Rei 36307-352, Brazil

✉ E-mail: demercil@dee.ufc.br

Abstract: This study introduces a low-cost topology used in a wind energy conversion system with efficient power control in order to meet battery charge requirements. The proposed structure is based on a high-frequency three-phase semi-controlled rectifier operating in the discontinuous conduction mode associated with a buck converter. The system comprises three control loops, which limit the current and voltage ratings to the maximum values allowed by the batteries and also regulate the voltage across the intermediate dc link. In addition, a novel maximum power point tracking algorithm that intends to maximise the power extracted from the wind turbine/generator/converter association is proposed. The principle of the proposed technique is based on a modified version of power signal feedback algorithm, where a given power level can be extracted from the wind turbine for each value of the mechanical speed. However, since the optimal power curve is not exactly known and temperature causes considerable variations in the optimal power curve, a method to search the best match is proposed. Experimental results from a 300-W prototype are presented and discussed.

1 Introduction

One of the major challenges in the control of any wind turbine lies in the wide range of wind speeds that occurs as the weather changes. Large wind farms choose their location carefully to reduce this influence, also aggregating complex turbine control and/or power interface systems that match the turbine operating condition according to the available wind speed to maximise the extraction of energy. Unfortunately, this is not adequate for low power turbines, because the installation site is usually determined by factors other than the wind profile, the generators are usually of permanent magnet synchronous type with fixed electrical characteristics, and cost and reliability are always a major constraint for low power renewable systems [1].

Considering that commercial battery chargers for small wind energy conversion system (WECSs) typically do not meet such requirements [2], a student competition sponsored by the Institute of Electrical and Electronics Engineers and the Power Electronics Society, that is, The 2009 International Future Energy Challenge (IFEC 2009) was proposed. The goal was the development of a power electronic converter interface for a WECS that could

- Support and protect the system operation under all operating conditions.
- Achieve maximum power transfer when charging a 12- or 24-V battery over a wide range of wind speeds without overcharging or damaging the battery.
- Provide reliable operation conditions without significant user support over many years of use.
- Be a leading edge solution in terms of improved performance, reliability and safety.
- Aggregate reduced dimensions associated to minimum component cost and count to minimise manufacturing cost per unit.

More specifically, a low cost power converter should be developed to maximise the energy extraction from a 300-W

domestic wind turbine system when operating over a wide range of wind speeds without damaging the battery, the generator and/or the turbine. Besides, manufacturing cost should be less than US\$20 at high-volume production, that is, approximately 100 000 units per year.

Considering the extensive review on power converter topologies for WECSs using synchronous generators in [3, 4], it has been found that some of them are feasible to small WECSs [5], which will be briefly described as follows. Although the direct connection of a three-phase rectifier to batteries has been a common practice adopted by some manufacturers, several problems associated with this solution result, such as the reduction of batteries useful life, increase of power losses, quasi-constant speed operation and limited wind speed range operation [6]. To allow operation with variable speed, the use of an intermediate dc–dc stage may be considered. Although a buck converter is employed in [7] for this purpose, energy extraction is only possible above certain value of the mechanical speed. Besides, a crowbar is necessary since electronic braking is limited because of the output voltage rating. A boost converter is used in [8] and energy extraction at low wind speeds is possible. However, since the output voltage limits the maximum mechanical speed, many batteries must be connected in series to allow wide speed range operation, which is a constraint in low power systems. To overcome the aforementioned drawbacks, a buck-boost converter is proposed in [9, 10]. Although wide speed range is possible, the current and voltage stresses in the semiconductors are somewhat high and efficiency is reduced if compared with similar approaches. A discontinuous conduction mode (DCM) three-phase single-ended primary inductance converter (SEPIC) topology is also proposed in [11]. Wide speed range operation and power factor correction (PFC) for the generator currents are achieved, thus reducing the generator losses. However, higher stresses regarding semiconductors and capacitors exist. A single-switch three-phase boost rectifier is employed in [12] with similar characteristics to those in [8],

although PFC is achieved in this case. To improve control flexibility, a three-stage approach with boost and buck converters was employed in [13]. Even though the optimum design of each conversion stage is possible, global efficiency is less than 90% because of three cascaded stages. A three-phase high-frequency semi-controlled rectifier was proposed in [14, 15] as a simple alternative to other conventional approaches with high component count [16]. This approach allows maximum power point tracking (MPPT) over a wide range of wind speeds, as well as limitation of the current through the battery. Since only two stages are used, increased efficiency is expected if compared with [13]. Partial PFC is possible with reduced total harmonic distortion (THD), that is, <20%. However, the size of input inductors does not make this solution feasible in practical applications. Although the use of a six-switch high frequency rectifier reduces the input filter requirements, the high side switches demand the use of complex drive circuitry [17].

Regarding the power extraction from the wind turbine, it is well known that there is an optimum angular mechanical speed for each wind speed rating, which then maximises the energy extracted from the wind [18]. A thorough review on MPPT techniques is presented in [19] and the main approaches are briefly reviewed as follows:

- (1) Tip speed ratio (TSR) control: The optimal TSR for a given wind turbine is constant and does not depend on the wind. Considering that TSR remains constantly at the optimal value, maximum power is extracted. In this method, the optimal TSR is compared with the actual wind speed. If some error exists, the speed of the generator is changed by the controller aiming to reduce it. The optimal point of the TSR can be determined experimentally or theoretically and stored as a reference [19]. Although this method seems rather simple as wind speed is directly and continuously measured, an anemometer must be used to measure it, as this method does not become feasible in small WECS because of the high cost and other practical issues [20].
- (2) Optimal torque control: This method relies on the adjustment of the permanent magnet synchronous generator (PMSG) torque according to a maximum power reference torque of the wind turbine at a given wind speed. In general, this method is simple, fast and efficient. However, efficiency is lower compared with other approaches, for example, TSR control because the wind speed is not measured directly, while wind changes are not reflected instantaneously and significantly on the control action [19, 20].

(3) Power signal feedback (PSF) control: Considering that the wind turbine characteristic is previously known and the mechanical speed is measured, a lookup table is used to give the optimum power or torque to be imposed for each speed [21]. If the power converter characteristic is known, some other variables, for example, the duty cycle can also be imposed. However, the performance of the aforementioned technique depends on the accuracy of the turbine model and can be also affected by parametric variations.

(4) Perturbation and observation (P&O) or hill-climb searching method: It is based on perturbing a control variable using a small step-size and observing the resulting changes in the target function until the slope becomes null [19]. Since the P&O method does not demand prior knowledge of characteristic curves, it is a far simple and flexible approach. However, it is not able to determine the maximum power point (MPP) when rapid wind variations occur in large and medium inertia wind turbines.

Considering the limitations of the aforementioned methods, this paper proposes a novel MPPT technique used in a small WECS based on a three-phase high-frequency semi-controlled rectifier operating in DCM.

2 Proposed WECS

The WECS in Fig. 1 is composed of a PMSG connected to a three-phase rectifier using three active switches and three diodes [14, 22, 23]. Since DCM operation is adopted, external film capacitors associated with the internal impedances of the electric generator L_1 , L_2 and L_3 are used to mitigate the high frequency current ripple. The dc-dc stage is a conventional buck converter. The main advantages of the proposed WECS when compared with other conventional approaches are [24]

- All switches in the rectifier stage are connected to the same reference node, thus simplifying the drive circuitry.
- There are not switches in series in the rectifier stage, thus eliminating the possibility of short-circuit through legs.
- There are only two conversion stages, with consequent increase of efficiency if compared with [14].
- The dc link voltage control and the step-up characteristic allow the operation at both low and high wind speeds.
- The controlled switches allow obtaining an electronically controlled braking system without the use of additional resistances or relays.

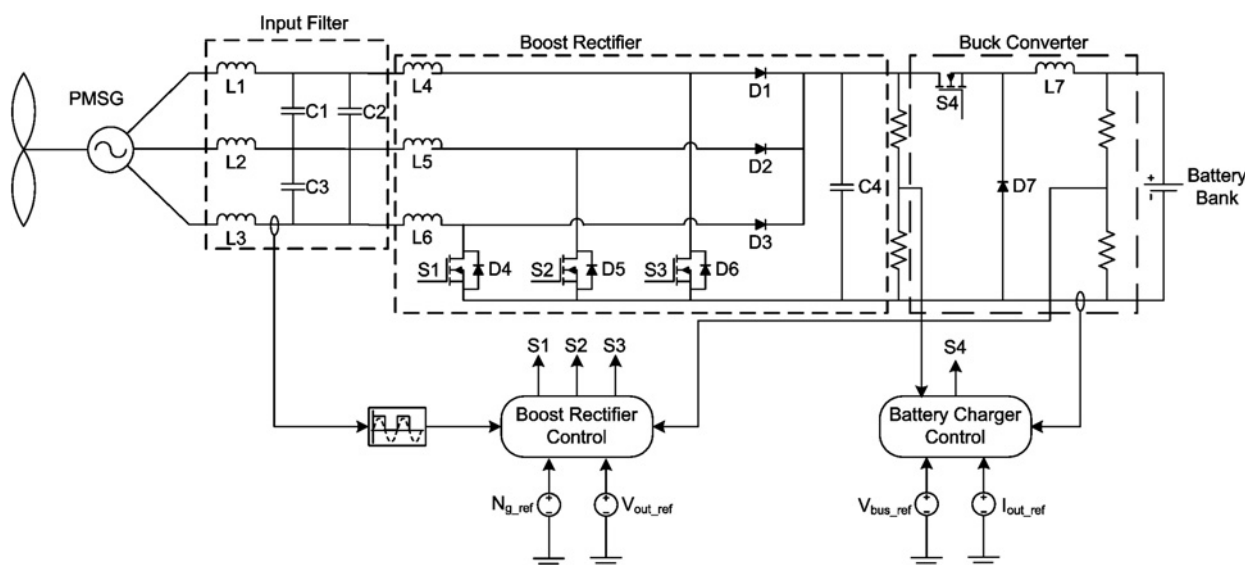


Fig. 1 High-frequency three-phase DCM semi-controlled rectifier associated with a buck converter

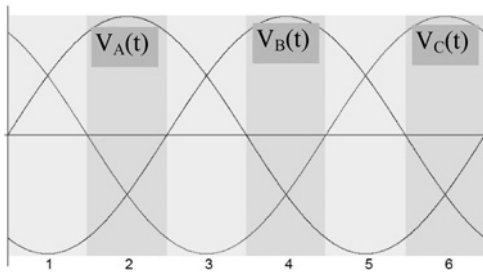


Fig. 2 Operational sectors according to voltages V_a , V_b and V_c

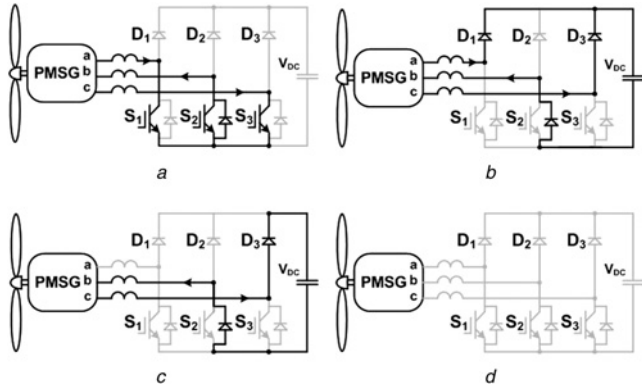


Fig. 3 Topological states and equivalent circuits associated to sector 1
 a First stage
 b Second stage
 c Third stage
 d Fourth stage

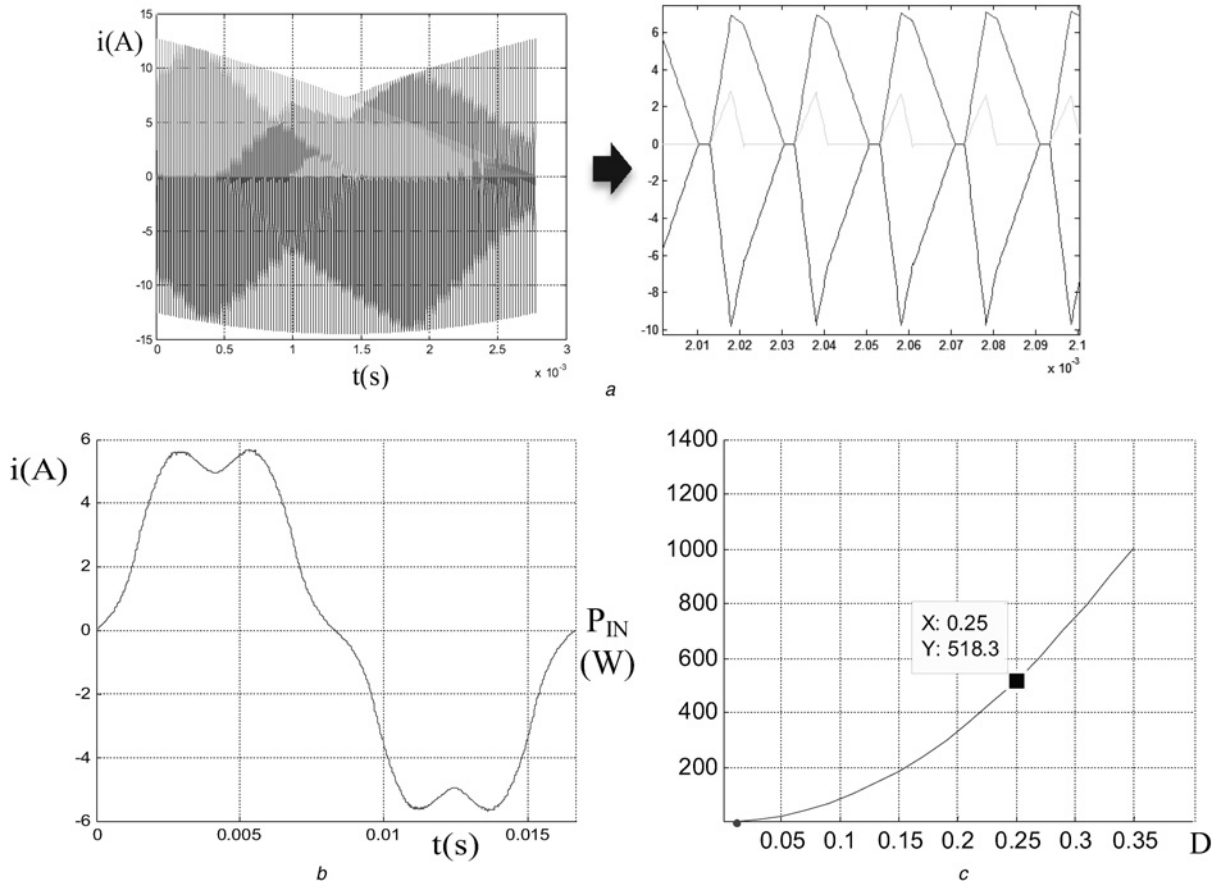


Fig. 4 Operation of the three-phase DCM semi-controlled rectifier
 a Envelopes and detailed view of the currents through inductors L_4 , L_5 and L_6
 b Filtered input current
 c Output power per phase of the PMSG as a function of the duty cycle

- DCM operation implies the reduction of dimensions of involved magnetics if compared with other topologies that operate in continuous conduction mode (CCM). Besides, there is no need of current sensors and additional control loops, while partial PFC occurs.

2.1 Operation of the DCM three-phase rectifier

The rectifier operates as a boost converter in DCM. When switches S_1 , S_2 and S_3 are turned on, current flows through them, while the currents through the respective inductors also increase. Diodes D_1 , D_2 and D_3 are reverse biased and capacitor C_4 provides energy to the buck stage. When switches S_1 , S_2 and S_3 are turned off, diode D_1 , D_2 and D_3 can be forward biased depending on the current direction, while energy is transferred to the load.

Fig. 2 shows that one cycle of voltages V_a , V_b and V_c can be divided in six sectors with similar behaviour and detailed as follows.

Sector 1: Voltages V_a and V_c are positive, while V_b is negative. When switches S_1 , S_2 and S_3 are turned on, line currents I_a and I_c increase linearly and flow through switches S_1 and S_3 , respectively, while line current I_b decreases linearly flowing through the anti-parallel diode of switch S_2 , as shown in Fig. 3. When switches S_1 , S_2 and S_3 are turned off, line currents I_a and I_c decrease linearly flowing through diodes D_1 and D_3 , respectively. Current I_b increases linearly flowing through the anti-parallel diode of switch S_2 , as shown in Fig. 3. When current either I_a or I_c becomes null, the remaining parameter becomes equal to I_b and the currents vary linearly until they become null. Fig. 4a shows that the currents through inductors L_4 , L_5 and L_6 become null, thus representing the operation in DCM. However, their respective envelopes are sinusoidal, which is a typical characteristic of the

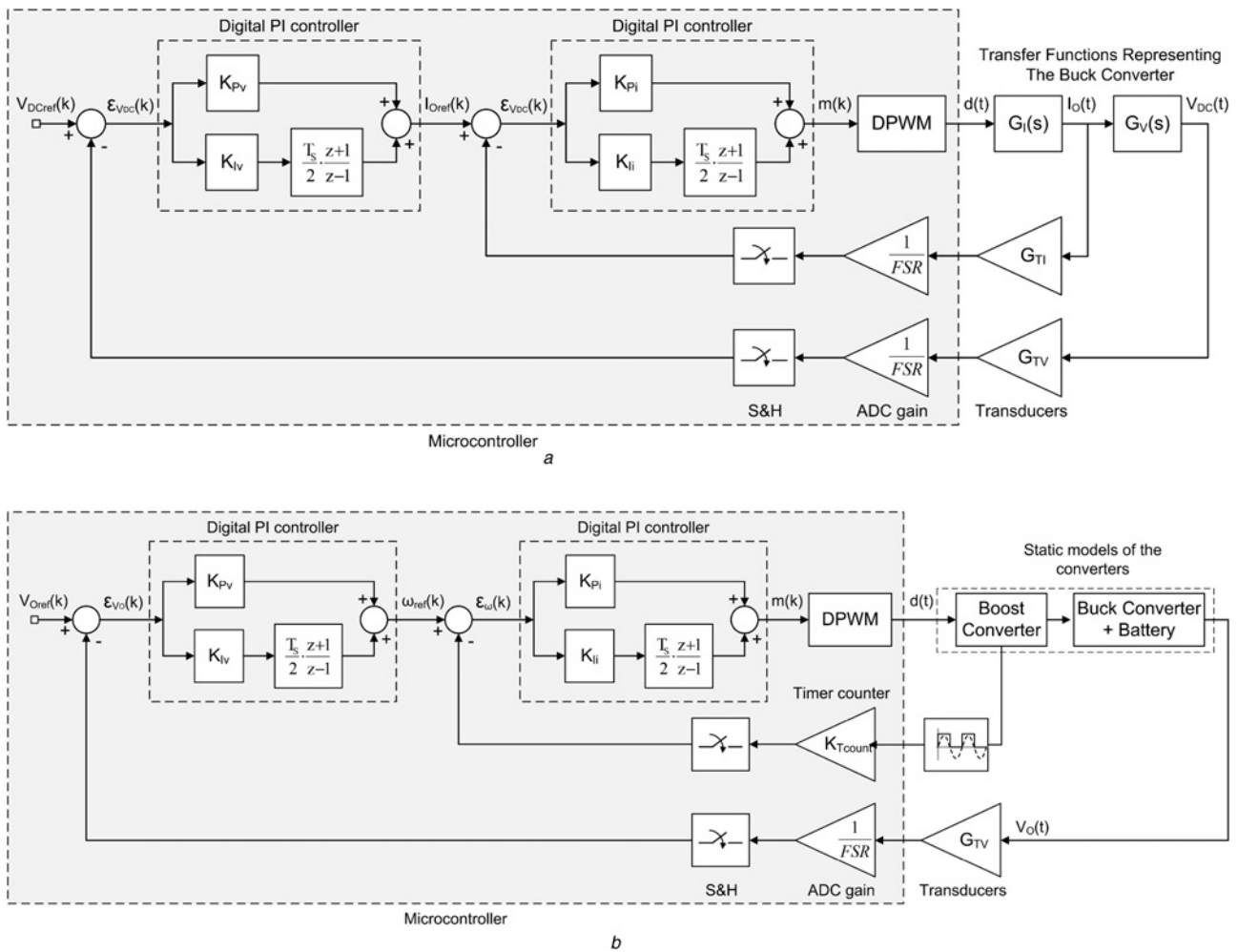


Fig. 5 Control system
 a Block diagram of the intermediate dc link voltage control loop
 b Block diagram of the battery voltage control loop

input current in rectifiers operating in DCM. Considering that the aforementioned waveforms are filtered, reduced distortion results as shown in Fig. 4b. Therefore the generator currents are nearly

sinusoidal without high frequency components because of their internal impedances associated with external capacitors C_1 , C_2 and C_3 , according to Fig. 4b.

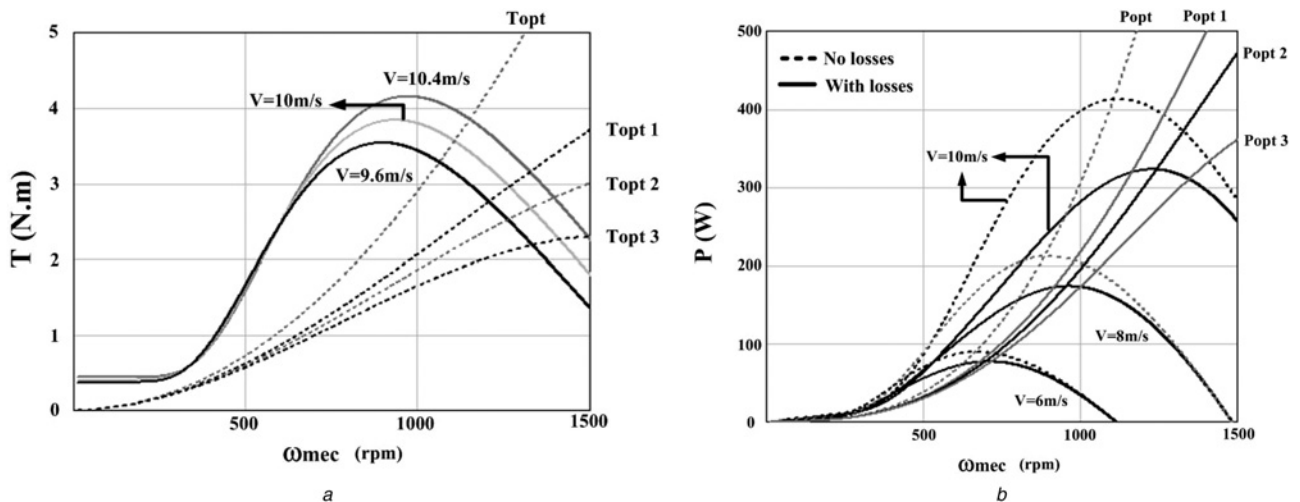


Fig. 6 Mechanical torque and mechanical power curves as a function of the rotational speed of the generator
 a Mechanical torque T_{mec} , ideal optimal mechanical torque T_{mec_opt} and optimal torque curves for different values of k_1 (T_{mec_opt1} , T_{mec_opt2} , T_{mec_opt3})
 b Mechanical power (P_{mec}), ideal optimum power (P_{mec_opt} , dotted lines), output power and optimal power curves for different values of a given constant k_1 (P_{mec_opt1} , P_{mec_opt2} , P_{mec_opt3})

The complete set of equations regarding the ac–dc stage allows plotting the instantaneous generator currents (Fig. 4b), the generator currents and the active power (Fig. 4c) as a function of the duty cycle. Besides, the active power can be obtained as (1), which can be determined without current sensing, where $k_v \omega_m$ is the phase voltage induced in the synchronous generator, D is the duty cycle, V_{dc} is the intermediate dc link voltage, L is the boost inductance and f_s is the switching frequency

$$P = 3 \frac{(k_v \omega_m D)^2}{2L f_s} \frac{V_{dc} / \sqrt{3}}{V_{dc} / \sqrt{3} - k_v \omega_m} \quad (1)$$

2.2 Control system

The following goals must be achieved by the control system for the accurate operation of the WECS:

- The voltage across the intermediate dc link represented by V_{C4} must remain constant.
- The maximum voltage and current ratings of the battery must be limited.
- Maximum power is supposed to be extracted from the wind turbine when the battery is not fully charged.
- The ac–dc boost converter operates in DCM, but the dc–dc buck converter operates in CCM.

Fig. 5a shows the control loop used to regulate the dc link voltage. An internal current loop limits the maximum charging current at the desired value. Although this control loop is always supposed to operate if an overvoltage across the dc link occurs, the rectifier switches are temporally turned on causing a short circuit in the generator and the wind turbine to brake.

Fig. 5b presents the battery voltage control system. If the battery voltage reaches the desired value, a digital proportional-integral controller reduces the rotational speed of the generator and the power extracted from the wind turbine is reduced, as the new operating point is not coincident with the MPP. The rotational speed can be measured by the frequency of the generator voltages or currents, being controlled by the duty cycle applied to the boost rectifier. If the battery is discharged, the rotational reference increases until the threshold value, which can be detected when the MPPT algorithm runs. When the battery is fully charged, the wind turbine is braked by short-circuiting it, which is a typical strategy used in small scale systems.

2.3 MPPT algorithm

The power available from the wind P_v and the mechanical power available at the rotor P_{mec} are given by (2) and (3), respectively, where ρ is the air density, R is the turbine radius, v is the wind speed, C_p is the power coefficient of the wind turbine, which depends on the TSR given by λ in (5)

$$P_v(v) = \frac{1}{2} \rho \pi R^2 v^3 \quad (2)$$

$$P_{mec}(\lambda, v) = C_p(\lambda) \cdot P_v(v) \quad (3)$$

$$\lambda = \frac{\omega_m R}{v} \quad (4)$$

From typical curves of C_p against λ , the optimum TSR λ_{opt} for a given wind turbine is constant and independent on the wind and rotational speeds as stated in (5)

$$\lambda_{opt} = \frac{\omega_{m_opt} R}{v} = \text{constant} \quad (5)$$

Substituting (5) in (2) and (3) gives (6), as it is possible to see that there is an optimum mechanical power for each rotational speed. It

is also worth to mention that conventional TSR control can be ideally based on expression (6) [19]. Fig. 6a shows the torque as a function of the rotational speed for different wind speeds and the torque for the optimum power curve T_{opt} as obtained in (7). Fig. 6b represents the respective mechanical power curves extracted from the wind and the optimum mechanical power curve

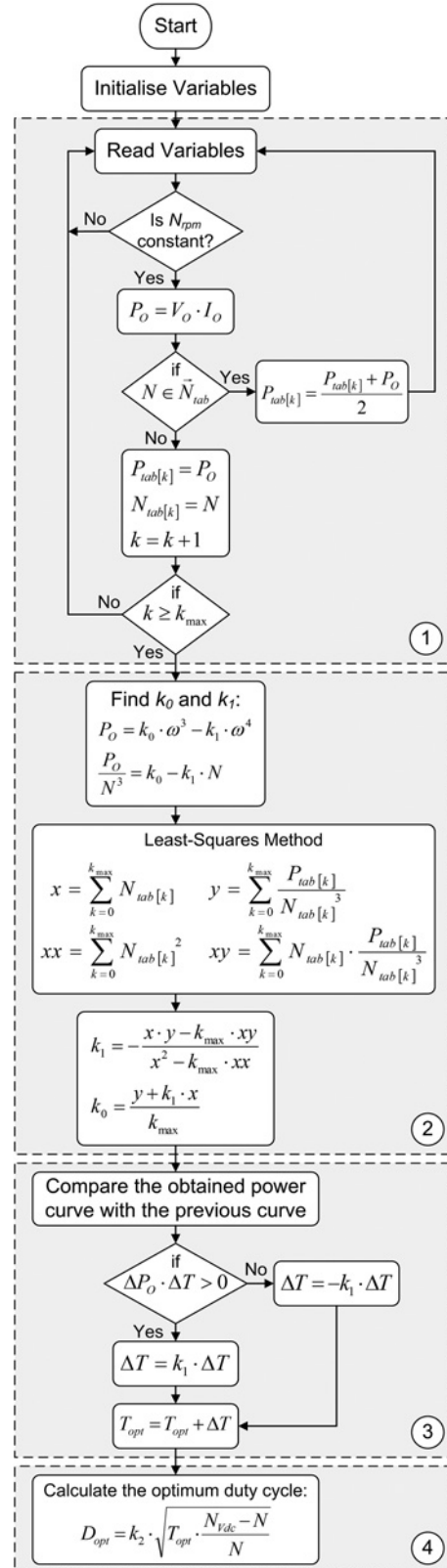


Fig. 7 Proposed MPPT algorithm

Table 1 Design specifications of the proposed WECS

Rms input voltage	$V_{LL} = 6-36 \text{ V}$
output voltage	$V_o = 24 \text{ V}$
switching frequency	$f_s = 50 \text{ kHz}$
output power	$P_o = 0-300 \text{ W}$
input power factor	0.96
THD of the input currents	19.5%

P_{opt} as dotted lines

$$P_{mec_opt}(\omega_m) = C_{p_opt} \cdot \frac{1}{2} \rho \pi R^2 \left(\frac{\omega_m R}{\lambda_{opt}} \right)^3 = k_{opt} \cdot \omega_m^3 \quad (6)$$

$$T_{mec_opt}(\omega_m) = k_{opt} \cdot \omega_m^2 \quad (7)$$

where C_{p_opt} is the optimum power coefficient of the wind turbine, k_{opt} is a given constant and T_{mec_opt} is the optimum mechanical torque.

However, the output power P_o delivered to the battery must take into account the losses in the generator and the power converter given in (8), where R_{eq} represents the equivalent resistance of the generator windings and the rectifier stage. Considering typical parameters used in small WECSs, the output power curves are shown as continuous lines in Fig. 6b. It can be seen that the influence of conduction losses is considerable as the maximum

output power occurs in higher rotational speeds than those for the maximum mechanical power

$$P_o(\lambda, v) = C_p(\lambda) \cdot P_v(v) - 3 \cdot R_{eq} \cdot I_{rms}^2 \quad (8)$$

where I_{rms} is the rms current through the generator windings.

Although the maximum extracted electrical power as a function of the mechanical speed cannot be obtained algebraically because of the nonlinear characteristic of the wind turbine, this paper proposes the approach indicated in (9) as a possible solution

$$P_{electrical_opt}(\omega_m) \simeq P_{mec_opt}(\omega_m) - k_2 \cdot T_{mec_opt}(\omega_m)^2 \quad (9)$$

where k_2 is a given constant.

Substituting (6) and (7) in (9), the maximum electrical power for each mechanical speed becomes

$$P_{electrical_opt}(\omega_m) \simeq k_0 \cdot \omega_m^3 - k_1 \cdot \omega_m^4 \quad (10)$$

Considering that k_0 is a typically known constant, the MPPT algorithm must determine the value of k_1 that generates the best output power curve. The curves P_{mec_opt1} , P_{mec_opt2} and P_{mec_opt3} considering three distinct values of k_1 are shown in Fig. 6b.

The proposed algorithm is based on modified PSF control, where a given power can be extracted from the wind turbine for each value of the mechanical speed. However, considering that the optimal

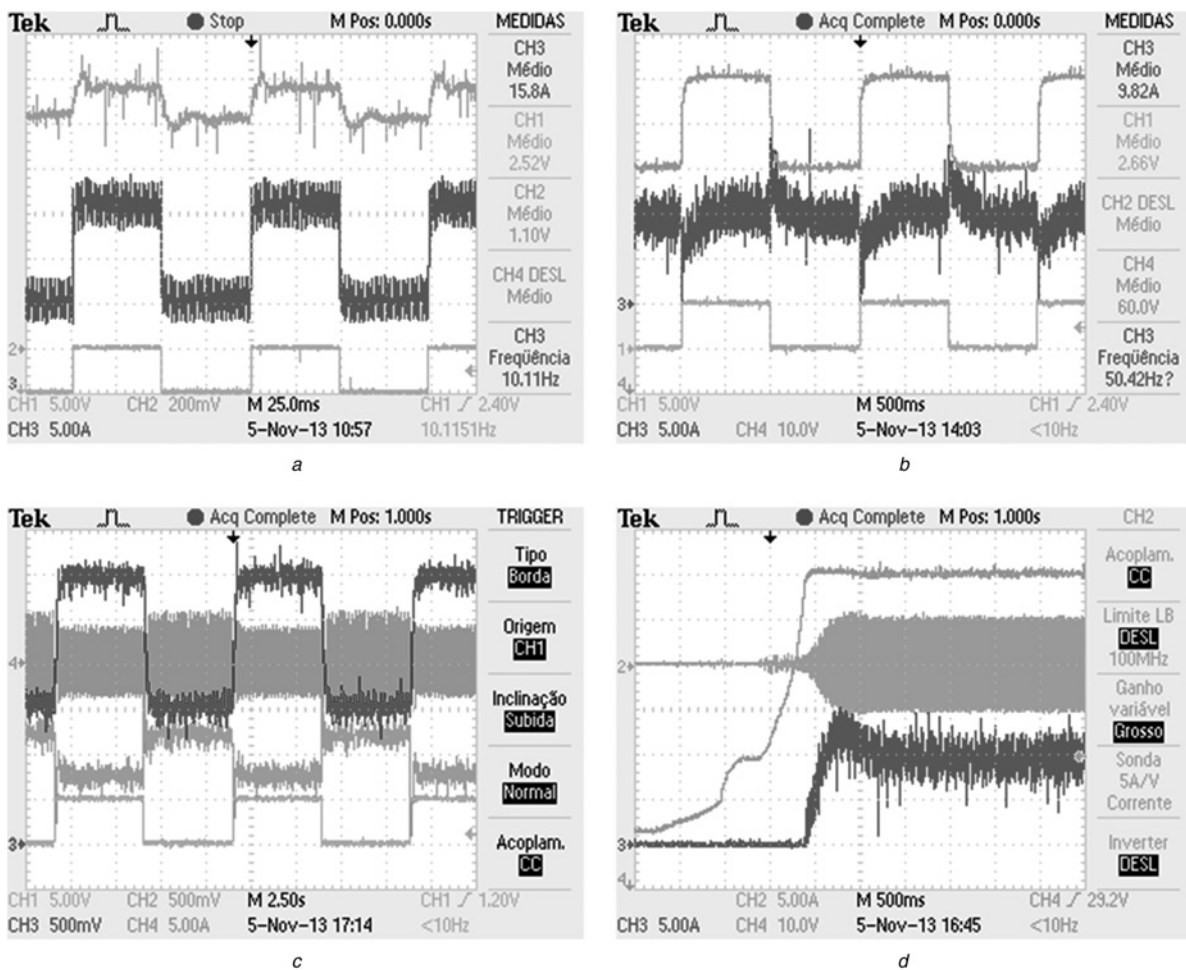


Fig. 8 Waveforms representing the dynamic behaviour of the proposed WECS

- a Duty cycle (upper trace – 5 V/div, 25 ms/div), output current (middle trace – 5 A/div, 25 ms/div) and reference current (bottom trace – 5 V/div, 25 ms/div)
- b Dc link voltage (upper trace – 10 V/div, 500 ms/div), output current (middle trace – 10 A/div, 500 ms/div) and voltage reference (bottom trace – 5 V/div, 500 ms/div)
- c Mechanical speed (upper trace – 33.3 rpm/div, offset of 300 rpm, 2.5 s/div), PMSG current (middle trace – 5 A/div, 2.5 s/div), duty cycle in the boost converter (middle lower channel – 10%/div, 2.5 s/div), speed reference (lower trace – 5 V/div, 2.5 s/div)
- d Dc link voltage (upper trace – 10 V/div, 500 ms/div), PMSG current (middle trace – 5 A/div, 500 ms/div) and output current (lower trace – 5 A/div, 500 ms/div)

power curve is not exactly known and temperature may influence k_1 significantly, aP&O approach is suggested to determine the best match for the power curve and described as follows. The main difference regarding the proposed method if compared with the traditional PSF control lies in varying parameter k_1 so that the extracted power can be maximised considering that parametric variations exist in the system.

According to Fig. 7, given an initial value of k_1 , an array is filled with data on the measured output power against rotational speed. To avoid the influence of the energy because of acceleration or deceleration, such measurements are valid only if constant speed occurs. Then, considering real wind conditions, some array positions are filled after a few minutes. Dividing the measured power by the cubed rotational speed causes the array to be linearised in the second stage of Fig. 7. The least squares method is then applied in the third stage, where coefficients k_0 and k_1 are obtained. The resulting power curve is then compared with a previous one (obtained with the previous value of k_1). This comparison must take into account a displacement in power curves in order to compare the obtained power for the same wind speeds. If the obtained power curve profile is improved of compared with the previous one, parameter k_1 is once again disturbed in the same direction. Otherwise, the disturbance occurs in the opposite direction. Therefore the proposed algorithm is able to provide the best power curve as well as to adapt this value considering parametric variations, which are mainly because of temperature.

3 Experimental results

The design specifications are shown in Table 1, leading to the design of an experimental prototype. Some relevant results are presented and discussed as follows.

3.1 Dynamic behaviour

A positive step in the reference signal causes the output current to increase from 10 A to 20 A as shown in Fig. 8a. It can be seen that overshoot is small and time response is <25 ms. Owing to the battery voltage variation, the duty cycle varies about 4%.

To validate the operation of the intermediate dc link voltage loop, a positive step is applied to the reference signal resulting in the waveforms shown in Fig. 8b. The dc link voltage is stepped up and down from 50 to 70 V and vice versa without overshoot, with a time response lower than 500 ms.

The mechanical speed control loop is validated considering a positive step in the reference signal from 400 to 500 rpm in Fig. 8c. Although no mechanical sensors are used, it can be stated that good step response without overshoot is achieved in <500 ms. Fig. 8d shows the forced startup of the wind turbine, where there are no additional stresses regarding the currents and voltages on the power converter.

3.2 Steady-state behaviour

The line voltage is maintained at $V_{LL} = 31$ V and the intermediate dc link voltage is $V_{dc} = 60$ V in the experimental tests, while some results are presented in Fig. 9 and discussed as follows. Fig. 9a shows that the output voltage is regulated at $V_o = 14.5$ V. The voltage across the active switch of the buck converter presents no overshoot and the current through the buck inductor is continuous with the expected ripple rating.

The waveforms regarding the boost converter operation in steady-state condition are shown in Figs. 9b and c. The current and voltage waveforms are as expected in theory, denoting the operation in DCM. The measured THD is 19.5% and power factor is 0.98. Although the current is nonsinusoidal, its respective harmonic content is quite reduced if compared with the conventional three-phase diode rectifier with capacitive filter.

The efficiency curves as a function of the output power are represented in Fig. 10a. Efficiency is about 88% at the maximum

power when a 24-V battery bank is used. Even though the achieved values are acceptable over the entire load range, efficiency can be improved by using a synchronous rectifier in the buck stage. The power factor curve is shown in Fig. 10b and it can be seen that this parameter remains higher than 0.97 over a wide load range as expected.

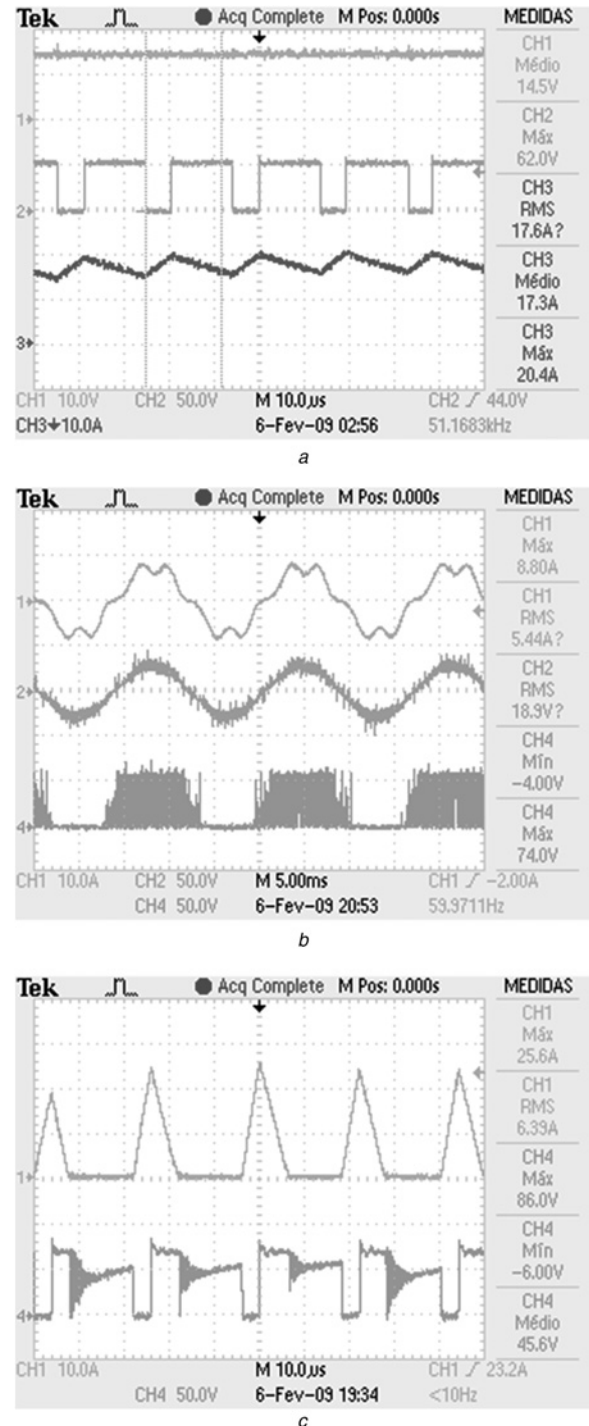


Fig. 9 Waveforms representing the steady-state behaviour of the proposed WECS

a Waveforms regarding the buck converter: output voltage (upper trace – 10 V/div, 10 μ s/div), voltage across the switch (middle trace – 50 V/div, 10 μ s/div) and current through the inductor (bottom trace – 10 A/div, 10 μ s/div)
b Waveforms regarding the boost converter: phase current (upper trace – 10 A/div, 5 ms/div), phase voltage (middle trace – 50 V/div, 5 ms/div) and voltage across one switch (bottom trace – 50 V/div, 5 ms/div)
c Waveforms regarding the boost converter: current through the input inductor (upper trace – 10 A/div, 10 μ s) and voltage across the switch (bottom trace – 50 V/div, 10 μ s)

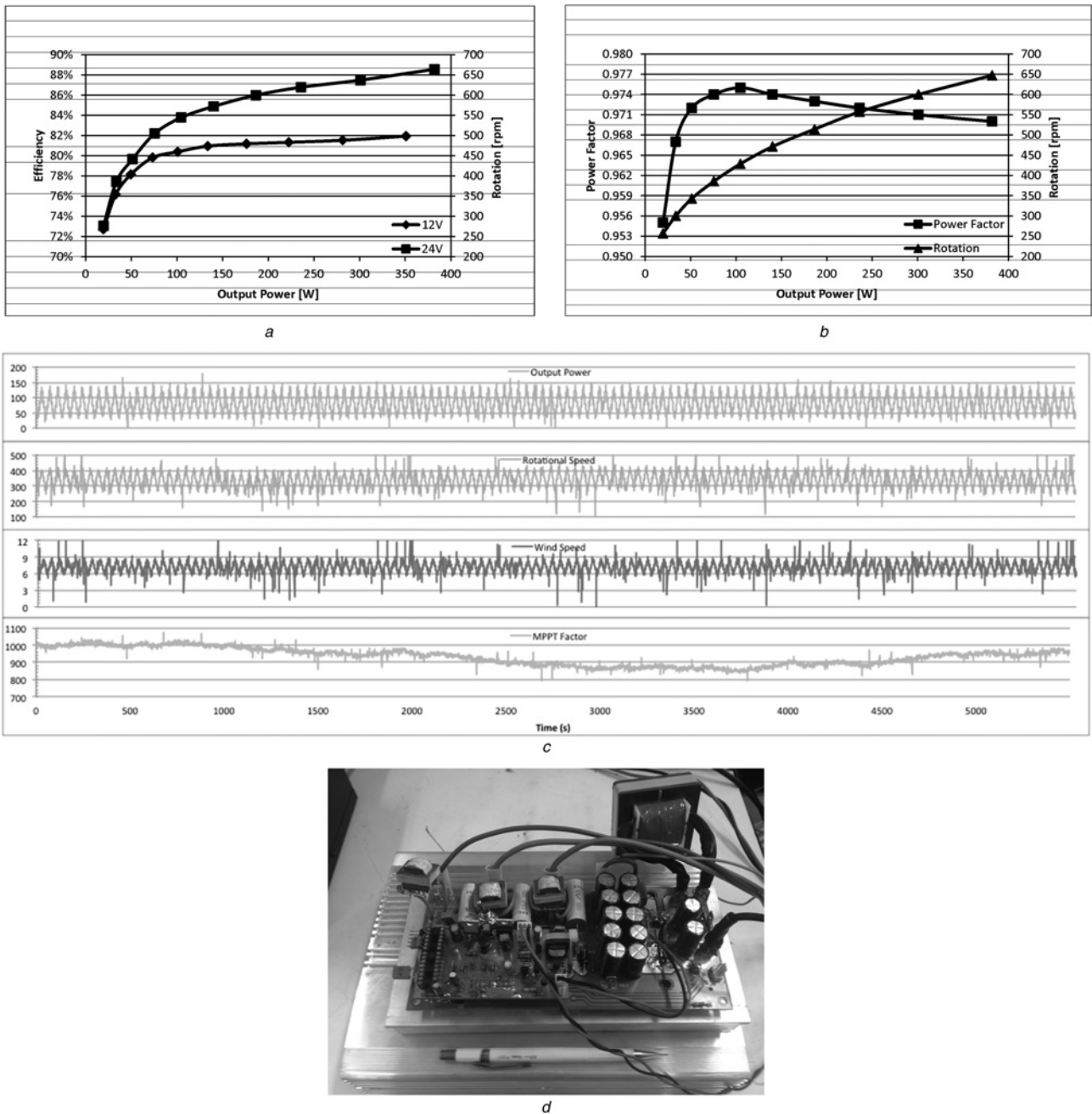


Fig. 10 Experimental results

- a Efficiency as a function of the output power
- b Power factor as a function of the output power
- c MPPT algorithm: output power, rotational speed, wind speed and MPPT factor
- d Experimental prototype

If compared with other solutions available in literature, the proposed WECS presents improved efficiency if compared with the approaches in [6, 7], where there is no PFC because a diode rectifier is used. Besides, considering the use of a buck-boost converter in [9, 10] and a SEPIC converter in [11], where higher current and voltage stresses exist, poor efficiency is also expected. Finally, it is reasonable to state that efficiency is higher in the introduced WECS because it uses only two power stages instead of three as in [13].

3.3 MPPT response

To validate the MPPT algorithm, a repetitive wind speed profile ranging from 6 to 9 m/s is applied according to the waveforms

shown in Fig. 10c. At $t=0$ s, an initial maximum power curve is followed. Then, after few dozens of seconds, the collected data are enough to allow the application of the least squares method in order to provide the normalised acquired power. A new curve is then generated and a new set of data is obtained, while the updated normalised power profile is compared with the previous one. Although the microcontroller limitations introduce some uncertainties and oscillations, it can be seen that the MPPT factor tends to decrease until a new steady-state value is achieved between 3000 s and 3500 s, as expected because of the increase of the windings temperature. At higher values of winding resistances, the output power can be increased with higher rotational speeds, where the voltages become higher and currents are lower. At $t=3700$ s, forced cooling is used in the PMSG. As the windings resistances decrease, the MPPT factor is increased

Table 2 List of components used in the experimental prototype

Quantity	Power stage element	Component	Description	Extended price, US\$
3	D_1, D_2, D_3	MUR420SG	ultrafast diode 200 V 4A Axial ON semiconductor	0.50
4	S_1, S_2, S_3, S_4	IRFP4710PBF	N-channel MOSFET 72 A/100 V	1.56
1	—	ACS713ELCTR-30A-T	hall effect sensor	1.54
3	C_1, C_2, C_3	B32232A1685 K	cap 6.8 μ F 100 V metal poly axial EPCOS INC	3.81
4	D_7	MBR20100CT	Schottky diode 20A/100 V	3.15
2	C_4	UHE2A471MHD6	cap 470 μ F/100 V elect he radial NICHICON	0.68
1	—	EEU-FC1H102B	cap 1000 μ F/50 V Elect FC Radial PANASONIC - ECG	0.40
2	C_4	ECWF2104JB	cap 0.1 μ F/250 V metal polypro PANASONIC - ECG	0.32
1	—	DSPIC30F2020	IC MCU flash 8KX14 W/Ad 14DIP microchip	3.97
2	—	LF347DRG4	amplifiers	0.44
3	L_4, L_5, L_6	NEE 20/10/5	ferrite core	2.85
1	L_7	NEE 55/28/21	ferrite core	2.00

and the system tends to operate close to the optimum TSR of the wind turbine.

3.4 Manufacturing cost

Table 2 shows the cost of each component used in the project considering high scale production as stated in the aforementioned contest. Besides, total cost is about US\$20.00. Even though high component count seems to be necessary for the prototype, dimensions are small as seen in Fig. 10d.

4 Conclusions

Despite the low cost and small size of the proposed converter, it is able to process the required power with acceptable efficiency and high power factor. A proper control strategy has been used to limit the voltage and current in the battery, thus preserving its useful life. The boost rectifier stage allows the extraction of power even at low wind speeds and the DCM operation allows the use of small size inductors with PFC and acceptable THD, thus increasing the overall system efficiency. Besides, it is worth to mention that the proposed WECS does not require dumps or emergency loads to protect the wind turbine against over speed. The components cost is estimated at about US\$ 20.00 as desired.

To optimise the power extraction, a MPPT technique that adapts the power curve used by the TSR control has also been proposed. Although satisfactory performance is achieved, it can be further improved by the investigation of wind speed estimation algorithms.

5 Acknowledgments

The authors acknowledge CAPES, FAPEMIG, CNPq and INERGE for the support to this work.

6 References

- Trilla, L., Bianchi, F.D., Gomis-Bellmunt, O.: 'Linear parameter-varying control of permanent magnet synchronous generators for wind power systems', *IET Power Electron.*, 2014, 7, (3), pp. 692–704
- Li, K., Xu, H., Ma, Q., Zhao, J.: 'Hierarchy control of power quality for wind-battery energy storage system', *IET Power Electron.*, 2014, 7, (8), pp. 2123–2132
- de Freitas, T.R.S., Menegaz, P.J.M., Simonetti, D.S.L.: 'Converter topologies for permanent magnetic synchronous generator on wind energy conversion system'. Proc. Brazilian Power Electronics Conf. (COBEP), 2011, pp. 936–942
- Jamil, M., Gupta, R., Singh, M.: 'A review of power converter topology used with PMSG based wind power generation'. Proc. IEEE Fifth Power India Conf., 2012, pp. 1–6
- Loh, P.C., Chai, Y.K., Li, D., Blaabjerg, F.: 'Autonomous operation of distributed storages in microgrids', *IET Power Electron.*, 2014, 7, (1), pp. 23–30
- Machado, I.R., Oliveira Filho, H.M., Barreto, L.H.S.C., Oliveira, D.S.Jr.: 'Wind generation system for charging batteries'. Proc. Brazilian Power Electronics Conf. (COBEP), 2007, pp. 371–376
- Guo, W., Wang, Y.: 'Simulation of a battery charging system with small wind power generator'. Proc. Seventh Int. Power Electronics and Motion Control Conf. (IPEMC), 2012, pp. 392–395
- Wang, H., Nayar, C., Su, J., Ding, M.: 'Control and interfacing of a grid-connected small-scale wind turbine generator', *IEEE Trans. Energy Convers.*, 2011, 26, (2), pp. 428–434
- Higuchi, Y., Yamamura, N., Ishida, M., Hori, T.: 'An improvement of performance for small-scaled wind power generating system with permanent magnet type synchronous generator'. Proc. 26th Annual Conf. of the IEEE Industrial Electronics Society, 2000, pp. 1037–1043
- Arifujaman, M., Iqbal, M.T., Quaicoe, J.E.: 'Maximum power extraction from a small wind turbine emulator using a dc-dc converter controlled by a microcontroller'. Proc. Int. Conf. on Electrical and Computer Engineering, 2006, pp. 213–216
- de Freitas, T.R.S., Antunes, H.M.A., de Freitas Vieira, J.L., Ferreira, R.T., Simonetti, D.S.L.: 'A DCM three-phase SEPIC converter for low-power PMSG'. Proc. 10th IEEE/IAS Int. Conf. on Industry Applications (INDUSCON), 2012, pp. 1–5
- Tonkoski, R., Lopes, L.A.C., dos Reis, F.: 'A single-switch three-phase boost rectifier to reduce the generator losses in wind energy conversion systems'. Proc. IEEE Electrical Power and Energy Conf. (EPEC), 2009, pp. 1–8
- de Oliveira Filho, H.M., Oliveira, D.S., de A. e Silva, C.E.: 'Three-stage static power converter for battery charging feasible to small wind energy conversion systems'. Proc. 10th IEEE/IAS Int. Conf. on Industry Applications, 2012, pp. 1–8
- Oliveira, D.S., Barreto, L.H.S.C., Antunes, F.L.M., Silva, M., Queiroz, D.L., Rangel, A.R.: 'A DCM three-phase high frequency semi-controlled rectifier feasible for low power WECS based on a permanent magnet generator'. Proc. Brazilian Power Electronics Conf., 2009, pp. 1193–1199
- Oliveira Júnior, D.S., Reis, M.M., Silva, C.E.A., Barreto, L.H.S.C., Antunes, F.L.M., Soares, B.L.: 'A three-phase high-frequency semiconverter for PM WECS', *IEEE Trans. Power Electron.*, 2010, 25, (3), pp. 677–685
- Su, B., Zhang, J., Wen, H., Lu, Z.: 'Low conduction loss and low device stress three-level power factor correction rectifier', *IET Power Electron.*, 2013, 6, (3), pp. 478–487
- Koutroulis, E., Kalaitzakis, K.: 'Design of a maximum power tracking system for wind-energy-conversion applications', *IEEE Trans. Ind. Electron.*, 2006, 53, (2), pp. 486–494
- Chen, Z., Guerrero, J.M., Blaabjerg, F.: 'A review of the state of the art of power electronics for wind turbines', *IEEE Trans. Power Electron.*, 2009, 24, (8), pp. 1859–1875
- Abdullah, M.A., Yatim, A.H.M., Tan, C.W., Saidur, R.: 'A review of maximum power point tracking algorithms for wind energy systems', *Renew. Sustain. Energy Rev.*, 2012, 16, pp. 3220–3227
- Tan, K., Islam, S.: 'Optimum control strategies in energy conversion of PMSG wind turbine system without mechanical sensors', *IEEE Trans. Energy Convers.*, 2004, 19, (2), pp. 392–399
- Wang, Q., Chang, L.: 'An intelligent maximum power extraction algorithm for inverter-based variable speed wind turbine systems', *IEEE Trans. Power Electron.*, 2004, 19, (5), pp. 1242–1249
- Singh, M., Khadkikar, V., Chandra, A.: 'Grid synchronisation with harmonics and reactive power compensation capability of a permanent magnet synchronous generator-based variable speed wind energy', *IET Power Electron.*, 2011, 4, (1), pp. 122–130
- Sharma, S., Singh, B.: 'Control of permanent magnet synchronous generator-based stand-alone wind energy conversion system', *IET Power Electron.*, 2012, 5, (8), pp. 1519–1526
- Almeida, B.R., Oliveira Júnior, D.S.: 'Power converter for vertical wind energy conversion system'. Proc. Brazilian Power Electronics Conf., 2013, pp. 468–473